10 μm imaging and HI observations of the Blue Compact Dwarf galaxy He 2-10[*]

M. Sauvage[1], T.X. Thuan[2,1], and P.O. Lagage[1]

[1] CEA, DSM, DAPNIA, Service d'Astrophysique, C.E. Saclay, F-91191 Gif-sur-Yvette Cedex, France
[2] Astronomy Department, University of Virginia, P.O. Box 3818, University Station, Charlottesville, VA 22903-0818, USA

Abstract. We have observed the Blue Compact Dwarf (BCD) galaxy He 2-10 in the ~ 10 μm mid-infrared (MIR) atmospheric window using broad-band filters centered at $\lambda 10.1$ μm and $\lambda 11.65$ μm. In both filters, only the galaxy's central regions were detected. One of the UV emitting regions is not detected, implying an older age. The central region contains two resolved components which have the same MIR properties but different Hα fluxes. We interpret these properties in terms of differing star forming histories. Based on its morphology, we show that the MIR emission is unambiguously associated with the young massive stars. We study the spatial variations of the MIR color and conclude that they imply the existence of a hot grain contribution to the 11.65 μm flux in the central regions of the starburst. We also present a new single-dish measurement of the HI content of He 2–10.

Key words: galaxies: individual: He 2-10 – galaxies: general – ISM: dust – infrared: galaxies – stars: formation

1. Introduction

Blue compact dwarf (BCDs) galaxies are low-luminosity ($M_{\rm B} \geq -18$) systems undergoing intense bursts of star formation in a very compact region, as evidenced by their blue UBV colors, and their optical spectra which show strong narrow emission lines superposed on a stellar continuum rising toward the ultraviolet, similar to spectra of HII regions (Thuan 1991). Their high HI content (Thuan & Martin 1981) and their low metallicity ($Z_\odot/50 \lesssim Z \lesssim Z_\odot/3$) suggest that BCDs are relatively "young" systems from the point of view of chemical evolution. Despite their low metallicity and dust content, IRAS has shown some BCDs to be strong mid and far infrared emitters

(Kunth & Sevre, 1985, Sauvage 1991), their dust being heated by an intense interstellar radiation field from the many massive stars in the starburst regions.

We present here 10 μm imaging and HI observations of the BCD He 2-10, which Conti (1991) has called a prototypical Wolf-Rayet galaxy. This galaxy was chosen because it has one of the highest IRAS 12 μm flux densities among BCDs (Sauvage, 1991). Moreover optical images (Corbin et al., 1993, hereafter CKV) and HST UV maps (Conti & Vacca 1994) have recently been obtained, to which the mid-infrared (MIR) observations can be compared. HI and CO maps of He 2-10 have also been recently published by Kobulnicky et al. (1995). Our MIR observations complement work at other wavelengths in several ways: 1) they suffer from little extinction as compared to the visible, 2) they have a much higher resolution ($\sim 1''$) than the IRAS observations (around $1'$), and 3) they allow to study the spatial distribution of the very hot dust as compared to that of the ionizing stars. We shall adopt hereafter a distance of 8.7 Mpc for He 2-10 (Tully 1988). At this distance, $1''$ corresponds to 42 pc.

2. Observations

2.1. MIR imaging

We have obtained three sets of observations for He 2-10. The BCD was first observed at the 3.6 m Canada-France-Hawaii Telescope (CFH) on April 22, 1992 with the Saclay-built CAMIRAS equipped with a 64×64 LETI/LIR Si:Ga array (Lagage et al., 1992) through the N (8-13 μm) filter. With a pixel size of $0.''45$ pixel^{-1}, CAMIRAS has a field of view of $\sim 29'' \times 29''$. The effective on-source time was 1130 s with an equal time on the OFF position to substract the background. The weather was fair and the Point Spread Function (PSF) derived from observations of the calibration star μUMa before and after the galaxy exposure is $1.''1$ Full Width at Half Maximum (FWHM). He 2-10 was reobserved in January 1993, during an effective on-source time of 1500 s, at the ESO 3.6 m telescope with TIMMI, the ESO 10 μm camera built at Saclay (Lagage et al., 1993), through the 11-12.5 μm filter (hereafter referred to as

the 11.65 μm filter). The scale was 0.″31 pixel^{-1}, giving a field of view of $\sim 20'' \times 20''$. The weather was non-photometric and the PSF, determined from reference stars observations was 0.″9 FWHM. We reobserved the galaxy at ESO on April 2, 1996 in the same configuration with photometric weather this time. The effective on-source time was 1355 s and the PSF 1.″5 FWHM.

During that last ESO run, target acquisition (He 2-10 and calibration stars) was performed by first slewing to a nearby SAO or Bright Star Catalog star with accurate coordinates, performing a re-adjustment of the telescope control system, and then offsetting to the target. We check using the calibration stars that the error in target position is always kept below 1″.

The observations were done using the standard chopping and nodding techniques. Typically 20 frames of 7.7 ms integration time each are taken in one position of the chopping mirror and summed. We perform 20 chopping cycles and subtract the OFF from the ON positions to create an image which is stored. Ten such images are created before the telescope is moved so that the ON and OFF beams are inverted. The number of such nodding cycles as well as the individual integration time are modified according to the intrinsic flux of the source and the desired signal-to-noise ratio. The chopping motions allow to substract the thermal emission from the sky as well as the spatially homogenous part of the telescope emission, while the nodding motions allow to remove residual emission from the telescope structure due to slight differences in the optical path for the two positions of the chopping mirror, as well as slow sky variations. The data were reduced using a software based on IDL developed at Saclay. Prior to any noise filtering processing, peak signal-to-noise ratios are 5.4 for the CFHT image, 7.2 for the 01/93 ESO image, and 6.5 for the 04/96 ESO image. The better S/N obtained during the 01/93 run is due to both the longer integration time and the use of a smaller pixel field of view that allows to operate the detector in nominal conditions.

The N-band filter has a central wavelength of 10.1 μm with half-power wavelengths of 7.7 and 12.8 μm (the transmission curves of all filters used here can be found on the ESO server at `http://http.hq.eso.org/proposals/ timmi.html`, the CFHT system being identical to the ESO one). Our image was calibrated using the standard star μUMa whose magnitude at 10.1 μm is -1.03 (Tokunaga 1984). Since the 10.1 μm flux density of a 0 mag star is 38 Jy (Abbot et al., 1984), assuming a spectral energy distribution going as $f_\nu \propto \nu$ (see Sect. 5.2), the total N-band flux density of He 2-10 is 1060 mJy, with an uncertainty of $\sim$10%.

The 11.65 filter has a central wavelength of 11.65 μm with half-power wavelengths of 10.8 and 12.5 μm. To calibrate the 11.65 μm image we used the stars λVel (N= -1.78) and αCen a (N= -1.56). We computed the expected flux densities of these calibrators at 11.65 μm assuming a stellar spectral energy distribution. Assuming again a spectral energy distribution going as $f_\nu \propto \nu$, we find a total 11.65 μm flux density of 850 mJy, with an uncertainty of 15%.

Two previous MIR photometric measurements of He 2-10 have been published. A low resolution map has been obtained by Telesco et al. (1993) who measured a 10.8 μm flux density

of only 600 mJy, with an uncertainty of 10-15%. As Telesco et al. (1993) made no spectral energy distribution correction for their measurement, i.e. they assumed a stellar energy distribution ($f_\nu \propto \nu^2$) for both the calibrators and the galaxy, we need to derive ours in the same conditions prior to any comparison. With a stellar energy distribution, our 10.1 μm flux density is only 970 mJy. This measure predicts a flux density of 850 mJy at 10.8 μm. This is only marginally consistent with the measurement of Telesco et al. (1993): 850 mJy $-$ 15% is 720 mJy while 600 mJy +15% is 690 mJy. The remaining discrepancy can probably be explained by the fact that (1) their detector pixels are spaced by more than their FWHM and thus do not fully sample the sky, and (2) He 2-10 is nearly resolved in their observation so that the correction to apply to the detected flux to obtain the true flux is difficult to deduce from the calibration star observations. If we assume that the signal loss is proportional to the sky undersampling, then the flux densities are in agreement. Cohen & Barlow (1974) have also observed He 2-10 in the N-band. They report a N magnitude of 3.5±0.2 within a 11″ diameter beam, which translates into a flux density of 1.6 Jy, higher than either our or Telesco et al. measurements. We believe that the difference cannot be due to a low level diffuse component as the more sensitive 12 μm IRAS measurement, with a beam covering the entire galaxy rather than just the star-forming regions, gives only a flux density of 1.1 Jy, lower than the Cohen & Barlow measurement, even after correction for the different bandwidths and taking into account the assumed IRAS spectral shape (see also our discussion in 5.2). Furthermore, using our images, we have simulated aperture photometry with an 11″ aperture and find no significant low-surface brightness component. We thus believe that measurement to be in error.

Figs. 1a and 2a show respectively the N and 11.65 μm images filtered with the multiscale maximum entropy method of Pantin & Starck (1996). The peak signal to noise ratio is now 30 in Fig. 1a and $\sim$100 in Fig. 2a. The initial difference in signal-to-noise ratio is amplified by the filtering process and also probably by the more compact nature of the emission at 11.65 μm. Note that the first contour in both images corresponds to approximately the same brightness level.

Spatial information at sub-arcsecond scale can still be restored with a deconvolution algorithm based on the same techniques. Figs. 1b and 2b show the deconvolved images. The FWHMs of these images are respectively 0.″8 and 0.″5 for the N and 11.65 μm images. Although they appear at a relatively high σ level, the structures seen East and South of region A in Fig. 2b are very likely artefacts of the deconvolution procedure.

2.2. 21 cm observations and the gaseous component

HI observations of He 2-10 were made with the NRAO[1] 43 m telescope at Green Bank on Nov 26, 1994, with a two-channel, dual polarization 21 cm prime-focus receiver with a system temperature of $\sim$20 K. The half-power beam width of the telescope
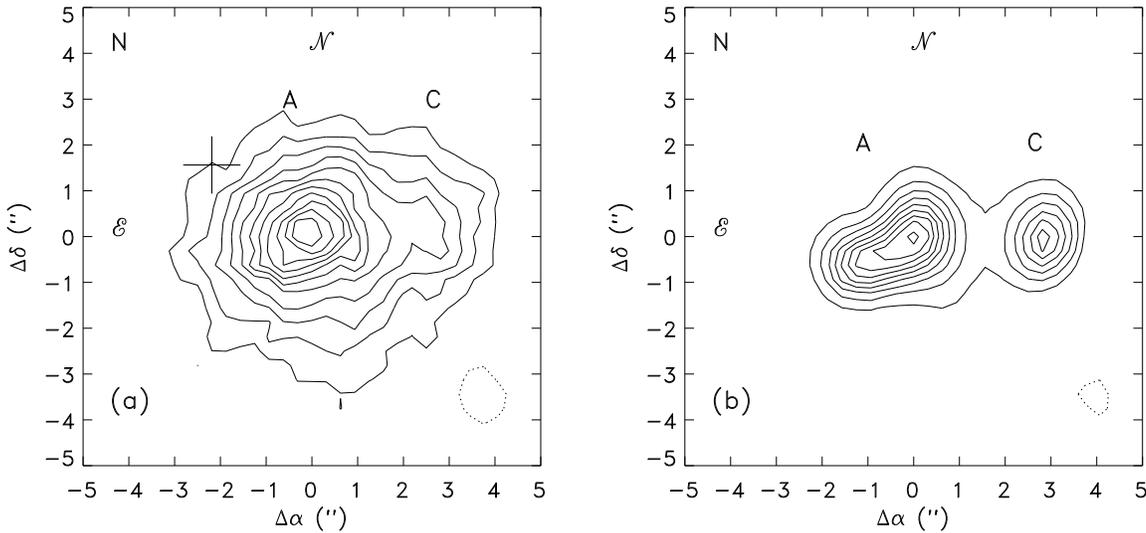

Fig. 1a and b. He 2-10 in the N-band filter, with labels of the star-forming regions following the nomenclature in the text. **a** Original image filtered with the multiscale, maximum entropy method of Pantin & Starck (1996). Contours start at 6σ and are spaced by 2σ (1σ is 2.2 mJy arcsec^{-2}). The dotted contour at bottom right is the FWHM contour ($1''\!.1$) of the PSF after a similar treatment. A cross in the upper left corner indicate the location of the CO peak observed by Kobulnicky et al. (1995). **b** Deconvolved image. The FWHM is now $0''\!.8$, shown as a dotted contour in the bottom right corner, and contours start at 5σ (as measured in the deconvolved image) and are spaced by 3σ.
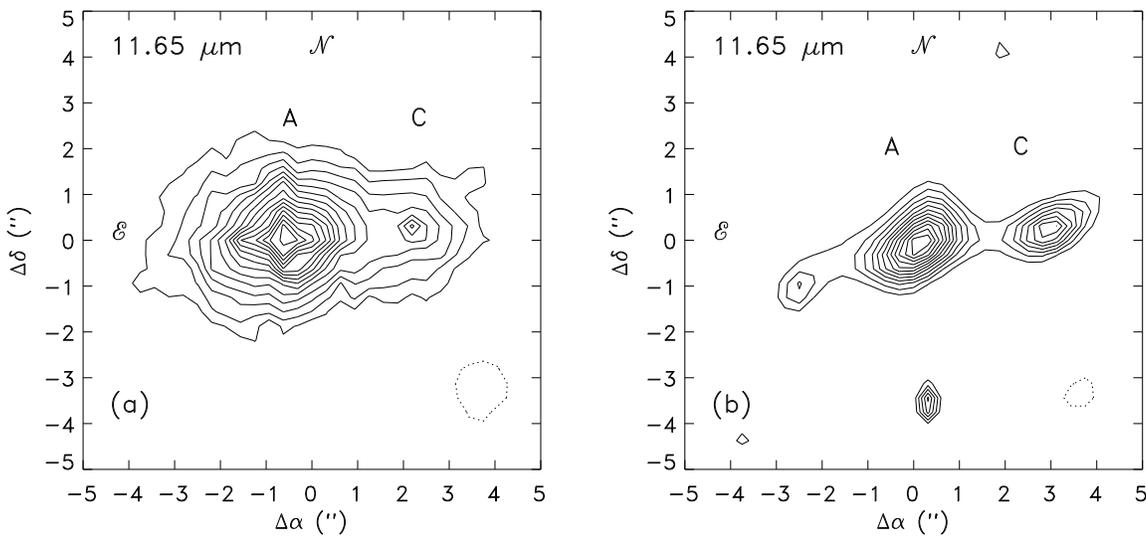

Fig. 2a and b. He 2-10 in the 11.65 μm band filter, with labels of the star-forming regions following the nomenclature in the text. **a** Original image filtered with the multiscale, maximum entropy method of Pantin & Starck (1996). Contours start at 12σ and are spaced by 6σ (1σ is 1 mJy arcsec^{-2}). The dotted contour at bottom right is the FWHM ($0''\!.9$) of the PSF after the same filtering treatment. **b** Deconvolved image. The FWHM is now $0''\!.5$, shown as a dotted contour in the bottom right corner, and contours start at 5σ (as measured in the deconvolved image) and are spaced by 3σ.

is $\sim 22'$. A bandwidth of 20 MHz was used with a 1024 channel autocorrelator split in two. The two polarizations were detected independently and averaged to improve sensitivity. The observations were made in the total-power position-switching mode, with 6 mn on-off integrations. Taking into account the two polarizations, a total integration time of 72 mn on source was obtained. The resulting spectrum is shown in Fig. 3. The effective resolution after Hanning smoothing is 16 km s^{-1} and a gain of

3.4 Jy/K was adopted. The derived H I parameters are: the heliocentric velocity $v_{\rm H} = 883 \pm 5$ km s^{-1}, the velocity width at 20% of peak intensity $\Delta v_{20} = 181 \pm 16$ km s^{-1}, the velocity width at 50% of peak intensity $\Delta v_{50} = 119 \pm 10$ km s^{-1} and the neutral hydrogen flux $F_{\rm HI} = 17.09 \pm 1.04$ Jy km s^{-1}. With a distance of 8.7 Mpc, the H I mass is $3.05 \pm 0.19 \ 10^8$ M$_\odot$. The peak flux density is 163 mJy, the rms noise is 8.8 mJy and the errors in

the velocity, velocity width, and flux density are calculated as in Schneider et al. (1990).

He 2-10 has been previously observed in H I by Allen et al. (1976) using the Parkes 64 m telescope with a $15'$ half-power beam width (HPBW). While there is a good agreement for v_H and the H I flux (the Allen et al. values are respectively 880 ± 20 km s^{-1} and 17.26 Jy km s^{-1}), our Δv_{50} is smaller and our peak flux density is higher (Allen et al. found 160 ± 20 km s^{-1} and 110 mJy).

Kobulnicky et al. (1995) have recently obtained a VLA H I map of He 2–10. They obtained an integrated H I flux of 9.87 ± 0.13 Jy km s^{-1}, only 58% of our value and a peak flux density of 90 mJy, only 55% of our value. As Kobulnicky et al., we interpret these differences as due to a low-intensity smooth outlying H I component resolved out by the interferometer. An extended population of 10^5 to 10^6 M$_\odot$ H I clouds lying in the periphery of the BCD will be missed. The VLA map gives a line center of 873 ± 10 km s^{-1} and a Δv_{50} of 106 ± 10 km s^{-1}, in good agreement with our values. The H I velocity field as seen with the VLA is consistent with solid body rotation, which results in a nearly gaussian shape of the H I single-dish profile as seen in Fig. 3. However, there is a definite asymmetry in the H I profile. There is a low-intensity wing on the high-velocity side which is not present on the low-velocity side. This asymmetry is also present in the VLA synthetic single-dish spectrum of Kobulnicky et al. (1995). Examination of the VLA H I total intensity and velocity maps shows that the high velocity component may be due to a distinct H I cloud to the north of the BCD. Solid body rotation in the interior part implies a mass distribution with a constant density in the inner 1.5 kpc radius. Adopting B_T = 12.45 (de Vaucouleurs et al., 1991), we obtain the distance-independent hydrogen mass to blue luminosity ratio $M(\mathrm{H\,I})/L_B = 0.25$ in solar units (to allow a direct comparison of this ratio to that measured for other galaxies, we have adopted here the convention expressing L_B in units of the Sun's blue luminosity, $L_B^\odot$; note that this differs from the convention used in Table 1, and that the ratio $L_\odot/L_B^\odot$ is ~ 6.25).

Kobulnicky et al. (1995) also obtained a ^{12}CO (1–0) map of the BCD. While the H I envelope is much more extended than the low-surface-brightness underlying elliptical stellar component (with colors typical of K-giant stars, Corbin et al., 1993) of the BCD, the CO emission is confined to a region of size comparable to that of the emission-line regions (see Corbin et al, 1993, their Fig. 2c), with however quite a different shape. The peak CO and H I brightnesses are separated by $\sim$500 pc. The Wolf-Rayet starburst is located between these two peaks, closer to the CO peak (see Fig. 1a). The H I map shows a hydrogen deficiency in the vicinity of the two starburst regions, which Kobulnicky et al. suggest may be the result of a replacement effect by molecular gas which fills this region. The CO data imply a total molecular gas mass of $1.6\pm0.1 \times 10^8$ M$_\odot$, assuming a Galactic CO-to-H$_2$ conversion factor. Thus the total gaseous mass is 4.7×10^8 M$_\odot$. The CO rotation curve implies that the mass of the young UV bright "proto globular clusters" discussed by Conti & Vacca (1994) can comprise up to half of the dynamical mass in the inner 70 pc radius. Both H I and CO maps show a tidal tail in the
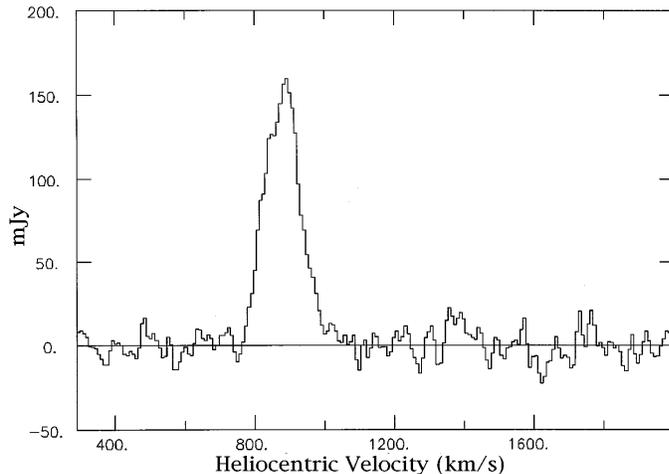

Fig. 3. 21 cm profile of He 2-10 obtained with the NRAO 43 m telescope at Green Bank.

SE direction, suggesting that He 2-10 is the product of a merger between two dwarf galaxies. However, the smooth $r^{1/4}$ profile of the underlying low-surface-brightness extended component (CKV) implies that it is a moderately advanced merger as the underlying stellar component has had time to relax. The total dynamical mass implied from the H I velocity field is 2.7×10^9 M$_\odot/(sin\,i)^2$ where i is the inclination angle of the BCD. Baas et al. (1994) have obtained a dynamical mass of $6.7\pm3.4 \times 10^9$ M$_\odot$ by extrapolation of the K-band flux. This would correspond to $i = 39°$. This inclination angle would give a M$_{dyn}$/L$_B$ ratio of ~ 5. Thus, unless the inclination is very low ($i \leq 10$ degrees), M$_{dyn}$/L$_B$ is relatively small, implying that most of the matter in He 2-10 is not dark but luminous (Lo et al., 1993). The corresponding gaseous mass fraction would be 0.07, somewhat on the low side of values for BCDs (Thuan 1985), a conclusion also reached by Baas et al. (1994).

3. MIR morphology

He 2-10 has been extensively imaged in the visible, both in broad and narrow band filters (Hutsemekers & Surdej 1984, CKV). The B and V images show high surface brightness irregular (i) star-forming regions in the central part of a more extended lower-surface-brightness elliptical (E) envelope, typical of the iE morphology defined by Loose & Thuan (1985). The color of the elliptical envelope is consistent with that of K giant stars (CKV).

Three starburst regions can be distinguished on the optical images. Following the nomenclature of CKV, the most prominent is region A at the center of the galaxy. Elongated in the SE-NW direction by $\sim 6''$ (FWHM) on B and V images, it is pointlike with a diffuse halo on Hα images (CKV). The second region is B, located at $\sim 8\rlap{.}''5$ E of A. It is smaller ($5'' \times 2''$) and fainter in B and V images and is seen at an even lower level in Hα. The third region, called C here, located $2\rlap{.}''7$ W of region A

Table 1. Observed and derived data on He 2-10.

Observed quantities		Derived quantities	
$\alpha_{1950.0}$	$08^h 34^m 07\overset{s}{.}1$		
$\delta_{1950.0}$	$-26°14'04''$		
redshift (km s^{-1})	883 ± 5	Distance (Mpc)	8.7
D_{25} ($''$)	104 ± 10		
R_{25} ($''$)	70		
m_B	12.45	L_B [2] (L$_\odot$)	$1.91\ 10^8$
$f(12\ \mu m)$ (Jy)	1.1	$L_{12\ \mu m}$ (L$_\odot$)	$3.5\ 10^8$
$f(25\ \mu m)$ (Jy)	6.55	$L_{25\ \mu m}$ (L$_\odot$)	$8.1\ 10^8$
$f(60\ \mu m)$ (Jy)	23.8	$L_{60\ \mu m}$ (L$_\odot$)	$1.47\ 10^9$
$f(100\ \mu m)$ (Jy)	25.7	$L_{100\ \mu m}$ (L$_\odot$)	$6.14\ 10^8$
		L_{FIR} (L$_\odot$)	$2.6\ 10^9$
$f(N)$ (Jy)	1.06 ± 0.1	L_N (L$_\odot$)	$(3.6\pm0.4)\ 10^8$
$f^A(N)$ (Jy)	0.71		
$f^B(N)$ (Jy)	< 0.1		
$f^C(N)$ (Jy)	0.35		
$f(11.65\ \mu m)$ (Jy)	0.85 ± 0.1	$L_{11.65}$ (L$_\odot$)	$(1.2\pm0.2)\ 10^8$
$f^A(11.65\ \mu m)$ (Jy)	0.57		
$f^B(11.65\ \mu m)$ (Jy)	< 0.1		
$f^C(11.65\ \mu m)$ (Jy)	0.28		
F_{HI} (Jy km s^{-1})[3]	17.09 ± 1.04	M_{HI} (M$_\odot$)	$(3.1\pm0.19)\ 10^8$
Δv_{50} (km s^{-1})[b]	119 ± 10		
		M_{H_2} (M$_\odot$)[4]	$1.6\pm\ 10^8$
		M_{gas} (M$_\odot$)	$4.7\ 10^8$
		M_{total} (M$_\odot$)[5]	$2.7\ 10^9/(\sin i)^2$
		$M_{dust}(IRAS)$ (M$_\odot$)	$7.6\ 10^4$
		$M_{dust}(\tau_{Si})$ (M$_\odot$)	$< 10.3\ 10^4$
		M_{HI}/L_B [6]	0.25
		M_{dust}/M_{gas}	$\lesssim 2.2\ 10^{-4}$
		M_{gas}/M_{total}	$0.17\ (\sin i)^2$

is not prominent in B and V images but is more noticeable in Hα and still more noticeable in [OIII].

In the MIR, only regions A and C can be seen. Region B, although within the field of view of the cameras, was not detected. We establish 3σ upper limits at the optical location of B of 8 mJy arcsec^{-2} in the N-band and of 3 mJy arcsec^{-2} in the 11.65 μm band, corresponding to upper limits for the total flux density of 80 mJy in the N band and 30 mJy in the 11.65 μm band, if we adopt for region B a MIR extent equal to its optical size of $5'' \times 2''$. We note that even when these upper limits are taken into account, our N-band measurement is still smaller than that of Cohen & Barlow (1974). Furthermore, it is not even clear if region B was inside the beam used by these authors.

The MIR morphologies are very similar in both N and 11.65 μm images: regions A and C are clearly resolved and separated. The peak-to-peak distance is $3''$, which corresponds to a linear scale of 126 pc. For region A the position angle remains approximately the same from N to 11.65 μm. This is not the case for region C, where there is a 45-90° rotation. The origin of this difference is unclear.

Apart from the extension of A, the MIR images are very similar to the Hα image, and even more to the [OIII] image of

CKV, implying that the dust responsible for the MIR emission is either coextensive with or closely connected woth the hot ionized gas responsible for the Hα and [OIII] emission. Our MIR images do not show evidence for a dust lane crossing the BCD North-South and separating regions A and B as hypothesized by Allen et al. (1976) and Hutsemekers & Surdej (1984).

Conti & Vacca (1994) have recently obtained 2200 Å images of He 2-10 with the Hubble Space Telescope (HST), where the emission regions are clearly resolved into sub-components. Region A is resolved into ~10 bright knots forming an arc, interpreted by the authors as proto-globular clusters (age$\lesssim$10 Myr). The SE-NW orientation of the arc is the same as that of region A in the MIR. The arc is ~ $2''$ long in the EW direction, thus is completely within region A. Region B is also resolved into several subcondensations, but instead of being ordered into an arc, the knots are scattered randomly throughout the region. The total UV luminosity of the knots in region B is 4 times fainter than that in region A. Region C is resolved into 3 knots with a total $L_\lambda(2200\ Å)$ luminosity about 20 times fainter than that of region A. It is interesting to note that the structure of region A observed in the UV by Conti & Vacca (1994) is more elongated than the Hα structure seen by CKV. The latter authors derive a diameter of $\lesssim$34 pc for the ionizing source, while the arc of stellar clusters observed by Conti & Vacca is ~85 pc long. A few clusters are resolved in the UV and their diameter is ~10 pc. It thus appears that only 1 or 2 of the UV clusters still contain massive ionizing stars.

Using the interferometric CO map of Kobulnicky et al. (1995), we can obtain a better picture of the starburst in He 2-10 by comparing the spatial distributions of the CO and MIR emissions. In Fig. 1a we show the position of the CO peak. It is located NE from the MIR peak, just on the lowest contour. The distribution of the CO gas is also slightly elongated, with the same position angle as region A in the MIR. This suggest that region A is actually located on the SE edge of the densest part of the CO cloud instead of just being seen projected against it. Region C, further to the W, is in a region of lower CO column density, while region B is completely outside the CO cloud on the other side.

A plausible way to bring together all the observations of He 2-10 in a coherent picture is the following: we are seeing in the BCD a photodissociation region resulting from the effect of a compact star-forming region on a neighboring CO cloud. Only the one or two youngest ($\leq 10^7$ yr) star clusters in the star-forming region still contain ionizing stars, which would explain the very compact aspect of the galaxy in Hα. However all star clusters are still young enough ($\leq 10^8$ yr) to produce copious amounts of UV radiation. This radiation photodissociates molecules in the nearby CO cloud as well as breaks up the larger grains or removes small dust grains from the mantles of the larger ones (e.g. Boulanger et al., 1990). H$_2$ emission is detected only to the East of region A (Baas et al., 1994) where most of the molecular gas is. He 2-10 has also been detected in [CII] with a flux of ~$2\ 10^{-14}$ W m^{-2} (S. Madden, private communication). If the [CII] and the H$_2$ S(1) 1-0 emission regions are coextensive, then their observed line intensity ratio

($\sim 10^{-3}$) can be explained by UV excitation of a gas with density 10^{2-3} cm^{-3} and an exciting radiation field 10^4 times more intense than the solar neighborhood radiation field (Hollenbach et al., 1991, Burton et al., 1992). However, given the very different beams used to observe these two emissions, it is quite likely that the H$_2$ emission is more concentrated than the [CII]. In that case shock excitation is required to produce the amount of detected H$_2$ emission. Such shocks are in fact to be expected in a starburst region. We note however that if the [CII] emission is spread out over the 55″ beam used to observe He 2-10, then its brightness is that expected from a classical photodissociation region with the density and radiation conditions mentioned above.

Thus this picture of a photodissociation region created by a very compact starburst located at the edge of a dense molecular cloud provides a reasonable description of all data available to date on the starburst in He 2-10. In that picture, the elongated morphology of region A in the MIR can be understood if the emitting dust is mixed with the UV clusters seen by Conti & Vacca (1994) or if the emission actually from the interface between the ionized region and the large molecular complex mapped by Kobulnicky et al. (1995), with a geometry reminiscent of the Orion Bar (e.g. Tielens et al., 1993, or Bregman et al., 1989). This geometry is in fact favored by the observation that there does not seem to be a large amount of material on the line of sight to the UV clusters (see Sect. 4).

4. Extinction

There exists several extinction estimates for region A. Using the Hα/Hβ ratio and case B recombination theory, Sugai & Taniguchi (1992, hereafter ST) derive a total (Galactic + internal) extinction of $A_V \sim 0.9$, while Vacca & Conti (1992) obtain $A_V \sim 1.7$ mag. With the Brγ measurement from Moorwood & Oliva (1988), we derive from the Brγ/Hβ ratio and case B recombination theory $A_V \sim 1.2$ mag, in good agreement with the optical estimates. The extinction from the Milky Way is $A_V \sim 0.6$ (Johansson, 1987), so that the intrinsic extinction in the optical is ~ 0.6 mag.

Aitken & Roche (1984) have, however, derived a much larger extinction $A_V \sim 10 \pm 5$ mag, using the optical depth τ_{Si} of the silicate absorption band at 9.7 μm. Adopting a Galactic ratio of molecular hydrogen column density to visual extinction, Kobulnicky et al. (1995) have derived from their CO map an even higher extinction $A_V \sim 30$ mag. Given that the CO cloud is not coexistent with the star-forming region, it is not surprising that the A_V derived from the CO data does not agree with the A_Vs derived from optical or MIR measurements. However, the large discrepancy between the optical and MIR A_Vs needs to be discussed.

We first note that the determination of the silicate absorption depth is not an easy task. The existence of two broad emission features on both sides of the silicate band (the 7.7 and 8.6 μm "blend" and the 11.3 μm band, see e.g. the ISOCAM spectrum in Boulade et al., 1996) makes it very difficult to locate the true level of the continuum, especially on the short wavelength side.

The difficulty in measuring τ_{Si} could explain why, in Phillips et al. (1984), five out of seven objects have an A_V as determined from silicate absorption larger than their A_V as derived from the Balmer decrement.

Alternatively, one could consider these discrepancies as real. Puxley & Brand (1994) have recently addressed the problem of extinction in the starburst galaxies NGC 1614 and NGC 7714 which, like He 2-10, show large discrepancies in extinctions measured at different wavelengths. They show that these measures can be reconciled if, instead of adopting a uniform foreground obscuring screen for the dust distribution, one assumes that the dust distribution is patchy. In that case, the shape of the absorption curve is such as to create an increasing bias for low extinction zones as wavelengths become shorter. Indeed, Fanelli et al. (1988) have found that in BCDs, the UV extinction is smaller than that derived from the Balmer decrement. They interpret the low UV extinction to be the result of a selection effect: UV radiation can only escape from regions where dust extinction is not large. A plausible origin for the patchy dust distribution is that the dust is efficiently destroyed or removed from the vicinity of O stars by the combined action of ionizing radiation, stellar winds and supernovae. This idea is supported by the HST observations of Conti & Vacca (1994) who estimate that region A contains ~ 30000 O stars within a diameter of ~ 90 pc (Schaerer, 1996, recently showed that this number may in fact be a lower limit to the true number of O stars in He 2-10). This corresponds to a very large energy density, comparable to that in the vicinity (~ 1.2 pc) of the central ionizing cluster of the Rosette nebula in the Milky Way. For the latter, a drop in the 12 μm emission is observed at that distance, which is presumably due to dust destruction by the intense radiation field (Cox et al., 1990).

Therefore, one can assume that in He 2-10, UV and optical light comes directly from the stellar clusters through holes in the gas and dust cloud. The MIR light, emitted preferentially at the photodissociation front (Tielens et al., 1993), i.e. deeper inside the cloud and projected at a different location on the sky, suffers from some extinction by foreground colder dust.

Because of the uncertainty in the true extinction and the poorly known shape of the MIR extinction curve, we have chosen not to correct the MIR measurements discussed here for extinction.

We note however that if we use $\tau_{Si} = 0.7 \pm 0.3$ (Aitken & Roche 1984) and the silicate absorption coefficient of Draine & Lee (1984), we derive a silicate mass of $5.1 \pm 2.2 \, 10^4 \, M_\odot$. If we further assume that silicates make up approximately one half of the total dust mass, we obtain a mass of $\sim 10.2 \, 10^4 \, M_\odot$, comparable to the value of $\sim 7.6 \, 10^4 \, M_\odot$ estimated from the IRAS FIR flux densities. This would correspond to a dust-to-gas mass (H I+H$_2$) ratio of $\sim 2.2 \, 10^{-4}$, as compared to $7 \, 10^{-3}$ in the solar neighborhood. Such a low value for the dust-to-gas mass ratio is not unusual for late-type dwarfs (Sauvage & Thuan 1994).

5. The interstellar medium and star-forming properties of He 2-10

5.1. Star formation

We now discuss the relationships between the 3 main star-forming regions in He 2-10.

B is by far the least active region: it has no MIR emission and only weak $H\alpha$ emission. This lack of MIR emission can be due either to a lack of hot stars (such as B stars, that do not produce ionizing emission yet are still quite efficient at heating the dust) or of dust. Since Conti & Vacca (1994) have seen stars clusters in region B with a total UV luminosity equal to 1/4 that of region A, we believe the second hypothesis to be the correct one. The lack of dust is also consistent with the absence of CO emission in region B (Baas et al., 1994). What is then the relationship between region A and B?

CKV have suggested that region A may have been the progenitor of region B, with star formation self-propagating from the former to the latter. We believe that this scenario is not consistent with our MIR observations, since we would then expect B to be currently forming stars. In that scheme, the weakness of the $H\alpha$ emission from B would have to be explained by a large dust extinction, but then we should have observed a large MIR flux, which is not the case. Furthermore, the location of region B outside of the CO cloud does not argue in favor of a large extinction on that line of sight. Region A could still have triggered region B if the burst duration in B was much shorter than that in A. But this is unlikely given that the oxygen abundance is 4 times larger in B than in A (Vacca & Conti 1992). To produce 4 times as much heavy elements than A in a shorter time, the burst in region B would have had to be much more intense than in region A, an unlikely possibility given that the gas density around region B seems to be much lower than toward region A. Thus it is more natural to think that region B, whose $(B - V)$ color is consistent with a population of mainly B stars, is older than region A. That B is older than A is also consistent with the burst ages derived from the $H\beta$ equivalent widths measured by Vacca & Conti (1992) and using the model of Viallefond & Thuan (1983). The age difference of only ~4 Myr, close to the shortest lifetime of supernovae progenitors, is probably too small to make plausible the hypothesis of a burst in A triggered by a burst in B. The location of the CO cloud between the two regions also does not support the hypothesis of shock waves propagating from B to A.

Because of its relative faintness in B and V images as compared to region A, region C has not often been discussed in the litterature. Yet it shows up clearly in $H\alpha$ and even more distinctly in [OIII] (CKV). We have shown in Fig. 4a the variation of the $H\alpha$ surface brightness along an EW cut through regions A, B and C as given by ST. The peak surface brightness of C is ~0.15 times that of A, and is similar to that of B. Fig. 4b shows the N surface brightness along the same cut and convolved to the same resolution, as derived from our images. Region C is now much brighter than B, which is not detected, with a peak surface brightness ~0.6 times that of A. Fig. 4c shows the re-sulting variation of the N/$H\alpha$ flux ratio, where region C has a N/$H\alpha$ ratio ~5.5 times greater than region A.

This change in the N/$H\alpha$ ratio can *a priori* be interpreted as indicating a higher extinction (by ~2.5 mag in V) in region C than in A, decreasing the $H\alpha$ emission relative to the N emission. However, we reject that hypothesis because (1) the $H\alpha$/$H\beta$ surface brightness profile given by ST suggests that the extinction is lower in C than in A and (2) the CO column density is much lower toward region C than toward region A.

A more likely interpretation is that C is smaller and younger than region A. Because it is smaller, it probably contains a smaller number of ionizing stars than region A, and hence has a smaller $H\alpha$ flux. But because it is younger, its heating spectrum contains relatively more UV photons than region A. Because of the shape of the absorption curve, these UV photons are more efficiently processed into mid-infrared photons by the dust, hence the larger N/$H\alpha$ ratio. That region C has a higher fraction of ionizing stars than region A is consistent with the higher $H\alpha$ equivalent width $W_\lambda(H\alpha)$ of C, $W_\lambda(H\alpha)$ varying according to the ratios 1.75:1.25:1 for regions C, A and B.

Region A is the dominant star-forming region of He 2-10. More than 2/3 of the total MIR radiation comes from it. Vacca & Conti (1992) estimate from the $H\alpha$ flux that it contains ~5000 O stars and 300 WR stars. These estimates are about a factor of 6 smaller than those derived from the UV 2200 Å luminosity by Conti & Vacca (1994). Given the very different light distributions, point-like in $H\alpha$ and extended in the UV, even after taking into account the different resolutions, this discrepancy implies that the $H\alpha$ emission comes only from a fraction of the UV knots. For example, if several of the UV knots are older than ~10 Myr, they would still produce appreciable $L_\lambda(2200\text{Å})$, but little Lyman continuum and hence $H\alpha$ emission (Conti & Vacca 1994).

5.2. Dust and the interstellar medium

We now use the MIR fluxes and colors to discuss the energy budget and nature of the dust in He 2-10.

To see whether the starburst in He 2-10 can power the whole infrared emission of the galaxy, we shall use the Rosette nebula as a template. Cox et al. (1990) derive a bolometric stellar luminosity of $2.23\ 10^6$ L$_\odot$. This estimate should be unaffected by extinction as it is based on the spectral types of the cluster stars. A FIR luminosity of $8.51\ 10^5$ L$_\odot$ is derived from IRAS maps giving a ratio of bolometric stellar luminosity to far infrared luminosity of $\simeq 2.6$. If we adopt the same ratio for He 2-10, we can reproduce the FIR luminosity of the galaxy: O5 stars in the $H\alpha$ emitting UV clusters in region A plus a 20 percent extra contribution from region C (see Fig. 4a) would account for a FIR luminosity of $\sim 1.6 \times 10^9$ L$_\odot$. As for the rest of the UV clusters (those that do not emit ionizing radiation), they would account for a FIR luminosity of 0.5-1.2×10^9 L$_\odot$. This results in a total of 2.1-2.8×10^9 L$_\odot$ while the FIR luminosity of the galaxy is 2.6×10^9 L$_\odot$. The starburst regions present in He 2-10 thus seem able to power the infrared emission of the galaxy.
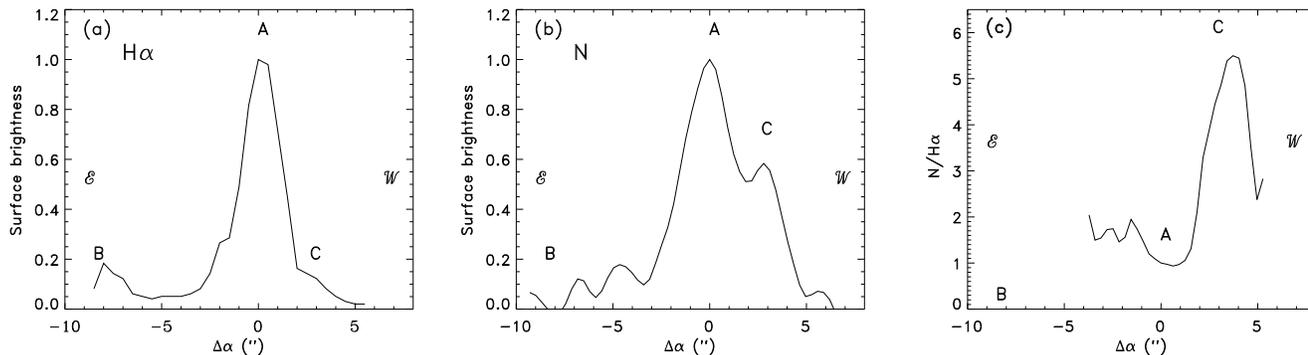
Fig. 4a–c. Surface brightness profiles in **a** Hα (from ST), **b** N, and **c** variation of the ratio N/Hα along an EW cut as defined in ST. The profiles are normalized to 1 at the location of region A. The N band data have been convolved to the resolution of the Hα data.

Since the global FIR luminosity of He 2-10 can be understood as powered mainly by the stars in the starburst regions, it is interesting to check whether these stars, O and early B stars mainly, can also account for the IR spectrum. To this end, we have used the 3-component dust models of Désert et al. (1990, the three components are PAHs, very small grains, and large grains) where the infrared spectrum is computed for various intensities of the heating field, this field being either that of an O5 star, that of a B3 star or the solar neighborhood one. We find that none of these models is able to reproduce the whole spectrum. Since the FIR emission is consistent with reprocessed OB stellar light, we first tried to make the O5 and B3 models fit the long-wavelength part of the IR spectrum. The result is that too much emission is predicted in the MIR range (by a factor 3 for the best fitting model). This could indicate that, relative to its large grain population responsible for the FIR emission, He 2-10 lacks small grains and PAH carriers because of its low metallicity (see the discussion in Sauvage et al., 1990).

To reproduce the short wavelength part of the spectrum with the models, we find that we systematically predict less FIR emission than what is actually observed in He 2-10. This may indicate an additional heating source, older stars for example, for the FIR emitting dust. However this hypothesis is somewhat in contradiction with the observation that the FIR emission can be deduced from the bolometric luminosity of the O and B stars in the starburst, assuming a conversion factor similar to that in the Rosetta nebula. It could be reconciled with that observation if (1) the true conversion ratio from O and B stars luminosity to FIR luminosity is lower in He 2-10 than in the Rosetta nebula, presumably because of a lower global dust abundance in He 2-10, and (2) the additional heating source by older stars is just the right amount as to make the observed ratio of bolometric OB stars luminosity to FIR luminosity equal to that observed in the Rosetta nebula.

Another possible explanation for the failure of the model to account for the observed spectral distribution is the reprocessing of the infrared emission inside the nearby molecular cloud, similar to the situation in M 17 (Gatley et al., 1979): the copious amounts of MIR radiation generated close to the UV clusters penetrate the molecular clouds and, depending on the MIR op-

tical depth, a significant fraction can be absorbed by dust and re-radiated in the FIR. To be efficient, this process requires a large amount of material, but the peak A_V of 30 measured by Kobulnicky et al. (1995) in the CO cloud indicates that this may be the case. As mentionned above, if the model of Désert et al. (1990) is to produce the FIR luminosity (60 and 100 μm), the MIR (12 and 25 μm) luminosity would be overestimated by a factor of $\simeq 3$. If we now require that the model only predicts $1/x$ of the observed FIR luminosity ($L_{\mathrm{FIR}}^{pred} = L_{\mathrm{FIR}}^{obs}/x$), where x varies between 1 and 3, the predicted MIR flux will be overestimated by $\simeq 3/x$ ($L_{\mathrm{MIR}}^{pred} = 3/x \times L_{\mathrm{MIR}}^{obs}$). To obtain the observed MIR luminosity, a fraction of $(1 - x/3)$ of the predicted luminosity has to be reprocessed in-situ to the FIR. In that case, the emerging FIR luminosity would be $L_{\mathrm{FIR}}^{pred} + (1 - x/3) \times L_{\mathrm{MIR}}^{pred}$. Given that in the model $L_{\mathrm{FIR}}^{pred}/L_{\mathrm{MIR}}^{pred} = 1.44$, one can solve for x so that the emerging FIR luminosity is equal to the observed one. We obtain $x = 1.4$. The optical depth required to reprocess 54% of the MIR luminosity is $\tau_{\mathrm{MIR}} = 0.8$. This value of τ has to be taken as an effective optical depth through the MIR band and is therefore less than the optical depth in the silicates band. Adopting $A_V/\tau_{\mathrm{Si}} = 19 \pm 1$ (Rieke & Lebovsky, 1985), we need $A_V \gtrsim 15$. It thus appears that internal reprocessing of the dust luminosity is the most likely explanation for the failure of the models of Désert et al (1990) to reproduce the observed infrared spectrum. A more definitive statement would require detailed radiative transfer calculations.

We now discuss how the [11.65 μm]-[N][7] color map of He 2-10 shown in Fig. 5 can constrain available MIR dust emission models. To construct the color map, we have used only the parts in the 11.65 μm and N images with a $S/N \geq 6$. Each image was smoothed with the PSF of its counterpart, thus the final resolution is a convolution of the ESO and CFH PSFs (approximately 2″ FWHM). It can be seen in Fig. 5 that the [11.65 μm]-[N] color varies from -0.23 at the edges to 0.0 at the location of the peak fluxes. The higher values (~ 0.03) toward the eastern edge of the map are probably an artefact of the interpolation algorithm used to superpose the individual maps
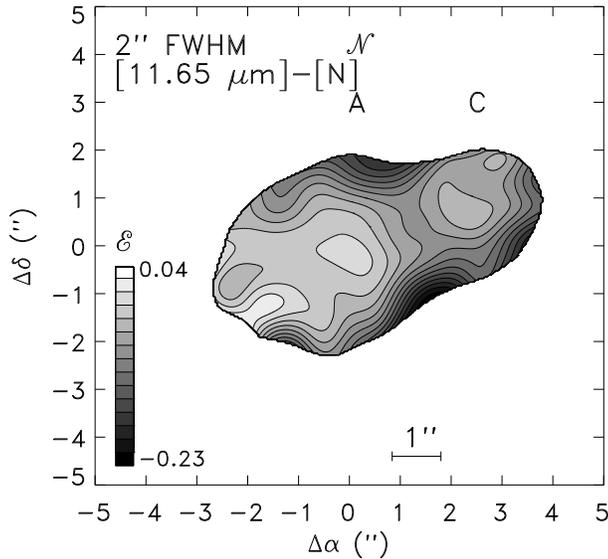
---

[7]   Here [X]= $\log f_\nu$(X).

Fig. 5. [11.65 μm]-[N] color map of He 2-10. Only the pixels with S/N$\geq$6 in both bands were used to produce the map. The color is minimum on the edges of the map (~ -0.23) and maximum (~ 0.0) at the location of the MIR emission peak. The contour interval is 0.02.

when computing the color map. The mean [11.65 μm]-[N] color of He 2-10 is -0.06.

To interpret the color map, we have built a simple synthetic model of the MIR spectrum made up by the sum of: 1) a continuum parameterized by n as defined by $f_\nu \propto \nu^{-n}$. This continuum has no physical basis and is simply a convenient parametrization to characterize the variations of the spectrum. 2) A silicate absorption band using the absorption efficiency of Draine & Lee (1984) and parameterized by the dust column density. 3) PAH emission bands, parameterized by the ratio of the 11.3 μm band flux to the N flux density, and 4) the NeII line, parameterized by the ratio of its flux to the N flux density. The mean values for parameters 2, 3, and 4 were obtained from Phillips et al. (1984) and Roche et al. (1991), while n was varied to obtain the best fit to the observed mean color. We get $n = -1$.

A priori, the task of deriving any useful information from the color map seems like a hopeless one, since we have a 4-parameter model for only two observational contraints, the mean color and its spatial variation. Fortunately, the last three parameters either induce color variations which are not in agreement with the observations or have little influence on the color. The color variation cannot be explained by a variation in the dust column density, since to reproduce an increase of the [11.65 μm]-[N] color towards the edges, the dust column density would have to be higher at the outskirts of the galaxy than at the center, which is nonsensical. This is due to the spectral shape of the silicate absorption coefficient, which decreases less steeply longward of 9.7 μm than shortward of it. As a result, increasing the dust column density decreases preferentially the 11.65 μm flux density.

As for the PAH emission bands present throughout the N bandpass, since in our simple model their ratios to the 11.3 μm band are fixed, they do not affect the [11.65 μm]-[N] color very much. Multiplying the flux of all the PAH bands by a factor of 100 results in a change of only -0.05 in the color. Relative band intensity variations could also be responsible for the color gradients. In the extreme case where only the 11.3 μm band is present, one still has to multiply its flux by 100 to produce a color variation of ~ 0.2. Such a multiplicative factor is highly unlikely, given the relative constancy of the 11.3/N flux ratio from galaxy to galaxy (Roche et al., 1991). Furthermore, it would be impossible to have colors smaller than the mean [11.65 μm]-[N] value (~ -0.06), given that the PAH flux is such a small fraction of the total flux in both the 11.65 μm and N bands (the flux ratio 11.3/N is 3.2×10^{-2} in He 2-10, Roche et al., 1991). The same reasoning applies to the NeII flux, the ratio of the latter to the N band flux being only $\sim 5.3 \times 10^{-2}$.

It thus appears that the shape of the "continuum" as parameterized by its slope n is the main factor controlling the color variation. Indeed, the full span of the colors seen in Fig. 5 can be reproduced by varying n from -3 at the outskirts of the map to 0 at the location of region A's peak. How are we to interpret this slope variation?

If we interpret it in terms of a single dust component made of thermalized grains, we run into a problem: the colors at the location of the peak MIR fluxes which are highest would be produced by dust at the coolest temperature, while the dust at the edges would be the hottest, a result which is <u>not</u> physical. The "continuum" slope variation could be explained by the existence of an increased emission at long wavelengths in the central regions of the map. This emission could come either from Very Small Grains (VSGs, Désert et al., 1990) or from warm coal grains (Papoular et al., 1993), i.e. a dust component not related to the PAH band carriers. This extra component would have its peak emission around 25 μm but would still noticeably affect emission toward 10 μm. As the intensity of the radiation field increases, the temperature of this extra dust component increases and its peak emission shifts to shorter wavelengths. Given that emission shortward of 10 μm is dominated by PAH bands, the net result of the higher radiation field would be a relative increase of the total dust emission on the long-wavelength side of the N band, mimicking the change in slope noted before. Such an interpretation has already been brought forward to explain the MIR colors of M 82 (see e.g. Telesco et al., 1990, their Fig. 13) and those of NGC 253 (Telesco et al., 1993). It can also be clearly seen in the spectra and images of star-forming regions obtained by ISO (see e.g. Vigroux et al., 1996).

Alternatively, these "continuum" slope variations could be explained by PAH-related variations. Indeed it is clear that even if the bands themselves contribute a relatively small fraction of the total MIR flux, some of them seem to be associated with much broader and intense features. This is the case of the 7.7 and 8.6 μm bands which are located on a very strong "bump" that is probably physically connected to them and that is providing most of the flux at these wavelengths. Thus the observed slope variation could be due to a variation of this bump's relative

contribution to the N-band flux density, its contribution being dominant in the outskirts of our map. This is plausible as in these outer regions, the radiation field is probably too low for emission other than that related to PAH carriers to be significant.

Finally we note that both mechanisms described above can actually be at work in He 2-10: in the central regions of the map, the UV flux is so intense that emission from very small grains appears in the 11.65 μm band and contributes to a flattening of the MIR spectrum. Away from these UV sources, this emission disappears from the 11.65 μm band while impulsive heating becomes the dominant mechanism and results in a spectrum dominated by the strong PAH blend around 8 μm. Furthermore, the mean index for the color of He 2-10 implies that this blend is a dominant feature of the spectrum, a property that could be related to the high mean UV flux density found in He 2-10. These conclusions can actually be checked by mapping this feature with ISO in Blue Compact Dwarf galaxies.

Since the above simple modelling of the spectral energy distribution in the MIR gives us a slope of the continuum emission in the 8-13 μm range, we can examine how our and the IRAS measurements compare. The 12 μm flux density of 1.1 Jy corresponds to a band-integrated flux of $1.5\,10^{-13}$ W m^{-2}. This is just the value we obtain by using our measured N band flux density and convolving the spectral ernergy distribution ν^{+1} with the IRAS bandpass. The good agreement implies that most of the MIR emission comes from the star-forming regions and that there is not a significant extended MIR diffuse halo, which would have been detected with the much larger beam of IRAS.

6. Conclusions

In this paper, we have presented the first high-resolution MIR images of the Blue Compact Dwarf galaxy He 2-10, as well as a new measurement of its H I content. Table 1 lists the general properties of He 2-10. Our conclusions can be summarized as follows:

1. The galaxy is detected and resolved into sub-components in the N-band and 11.65 μm filters. The main component, region A, at the center of the galaxy, is elongated in the SE-NW direction and has the same position angle in both MIR images. The same shape and orientation are also seen in the optical. The arc of UV clusters seen by Conti & Vacca (1994), and the Hα emitting region detected by Sugai & Taniguchi (1992) are contained entirely within the MIR emission of region A. The latter emits $\sim 2/3$ of the MIR flux of the galaxy. The second bright optical region of He 2-10, region B, at 8$''$5 E of region A, is not detected. A third region, C, appearing in the optical as a small H II region 2$''$7 W of region A, is clearly detected. Both regions A and C are at the edge of a very dense CO cloud.

2. The present star formation activity is very different from one region to the other. Region A is the most active, as is evident from its high Hα, UV and MIR fluxes. It is younger than region B: though the latter contains UV emitting stars, ionizing stars have died and most of the interstellar medium has been exhausted, as evidenced by the lack of CO emission.

We attribute the lack of MIR emission to a lack of dust rather than to a lack of heating flux. Region C, although smaller and less luminous in Hα than region A contains a higher proportion of ionizing to non-ionizing stars, as shown by its N/Hα ratio, which is 5.5 times higher than that of region A. We show that this difference cannot be attributed to a higher extinction, and probably reflects the younger age of region C.

3. We found that the large-beam 12 μm IRAS measurement is similar to our narrow-beam measurements, implying that there is no diffuse MIR emission. The UV-emitting clusters provide enough energy to heat all the dust emitting in the FIR. We show that the models of Désert et al. (1990) are however unable to fully account for both the observed MIR and FIR spectra. The model predicts too much MIR emission relative to the FIR emission. One possible way for reconciling the models' predictions with the observations is to invoke reprocessing of the MIR emission into FIR emission by dust close to the UV clusters, inside the very large molecular complex to the west of the starburst, where a very high extinction has been found.

4. We found comparable estimates for the dust mass using either the 60 and 100 μm IRAS flux densities or the silicate absorption depth. In both cases, the dust mass is $\sim 8\,10^4$ M$_\odot$. The corresponding dust-to-gas mass ratio is $\sim$ 16 times smaller than in the solar neighborhood but is typical of other BCDs.

5. The MIR color variations imply either that, in addition to PAH band carriers, there is an extra-component of very small grains with peak emission at $\sim 25\,\mu$m contributing in the hottest regions of the galaxy, or that the PAH "blend" of the 7.7 and 8.6 μm band strongly increases relative to the rest of the MIR emission toward the outskirts of the galaxy. A combination of these two mechanisms is actually quite likely. Furthermore, the mean color of He 2-10 is characteristic of a spectrum where this PAH "blend" at short wavelengths (7.7 and 8.6 μm) is dominant relative to the 11.3 μm feature. This is probably due to the high UV flux density found in He 2-10.

6. Our new H I measurement shows that He 2-10 has a gas mass fraction on the low side of the range for BCDs.

References

Abbot, D. C., Telesco, C. M., Wolff, S. C. 1984, ApJ 279, 225

Aitken, D. K., Roche, F. P. 1984, MNRAS 208, 751

Allen, D. A., Wright, A. E., Goss, W. M. 1976, MNRAS, 177, 91

Baas, F., Israel, F. P., Koornneef, J. 1994, A&A 284, 403

Boulade, O., Sauvage, M., Altieri, B., Blommaert, J., Gallais, P. et al. 1996, A&A, 315, L85

Boulanger, F., Falgarone, E., Puget, J.L., Helou, G. 1990, ApJ, 364, 136

Bregman, J.D., Allamandola, L. J., Tielens, A. G. G. M., Geballe, T. R., Witteborn, F. C. 1989, ApJ, 344, 791

Burton, M.G., Hollenbach, D.J., Tielens, A.G.G.M. 1992, ApJ, 399, 563

Cohen, M., Barlow, M. J. 1974, ApJ, 193, 401

Conti, P. S. 1991, ApJ 377, 115

Conti, P. S., Vacca, W. D. 1994, ApJL 423, L97

Corbin, M. R., Korista, K. T., Vacca, W. D. 1993, AJ 105 1313 [CKV]

Cox, P., Deharveng, L., Leene, A. 1990, A&A 230, 181

Desert, F.X., Boulanger, F., Puget, J.L., 1990, A&A, 237, 215

Draine, B. T., Lee, H. M. 1984, ApJ 285, 89

Fanelli, M. N., O'Connell, R.W. & Thuan, T.X. 1988, ApJ, 334, 665

Gatley, I., Becklin, E.E., Sellgren, K., Werner, M.W. 1979, ApJ, 233, 574

Hollenbach, D.J., Takahashi, T., Tielens, A.G.G.M. 1991, ApJ, 377, 192

Hutsemekers, D., Surdej, J. 1984, A&A 133, 209

Johansson, I. 1987, A&A 182, 179

Kobulnicky, H. A., Dickey, J. M., Sargent, A. I., Hogg, D.E., Conti, P. S. 1995, AJ, 110, 116

Kunth, D., Sevre, F. 1985, in *Star-forming dwarf galaxies and related objects*, Eds. D. Kunth, T.X. Thuan, J.T.T. Van, (Paris:Editions Frontiéres), p332

Lagage, P. O. et al., 1992, 42nd ESO conference, M.H. Ulrich (Ed.) p601

Lagage, P. O. et al., 1993, in *Infrared detectors and Instrumentation*, SPIE Conf., 1946

Lo, K.Y., Sargent, W.L.W., Young, K. 1993, AJ, 106, 507

Loose, H. H., Thuan, T. X. 1985, in *Star Forming Dwarf Galaxies and Related Objects*, ed. D. Kunth, T. X. Thuan, and J. T. T. Van (Gif-sur-Yvette:Editions Frontières), 73

Moorwood, A. F. M., Oliva, E. 1988, A&A 203, 278

Pantin, E., Starck, J.L. 1996, A&AS, 118, 575

Papoular, R., Breton, J., Gensterblum, G., Nenner, I., Papoular, R. J., Pireaux, J.-J. 1993, A&A 270, L5

Phillips, M. M., Aitken, D. K., Roche, P. F. 1984, MNRAS, 207, 25

Puxley, P. J., Brand, P. W. J. L. 1994, MNRAS 266, 431

Rieke, G.H., Lebovsky, M. J. 1985, ApJ, 288, 618

Roche, P. F., Aitken, D. K., Smith, C. H., Ward, M. J. 1991, MNRAS 248, 606

Sauvage, M., 1991, Thèse de doctorat de l'Université Paris-VII

Sauvage, M., Thuan, T. X. 1994, ApJ 429, 153

Sauvage, M., Thuan, T.X., Vigroux, L. 1990, A&A, 237, 296

Schaerer, D. 1996, ApJ, 476, L17

Schneider, S. E., Thuan, T. X., Magri, C., Wadiak, J. E. 1990, ApJS 72, 245

Sugai, H., Taniguchi, Y. 1992, AJ , 103, 1470 [ST]

Telesco, C.M., Campins, H., Joy, M., Dietz, K., Decher, R. 1990, ApJ 369, 135

Telesco, C. M., Dressel, L. L., Wolstencroft, R. D. 1993, ApJ 414, 120

Thuan, T. X. 1985, ApJ 299, 881

Thuan, T. X. 1991, in *Massive Stars in Starbursts*, ed. C. Leitherer, N. R. Walborn, T. M. Heckman and C. A. Norman (Cambridge:Cambridge University Press), 183

Thuan, T. X., Martin, G. E. 1981, ApJ 247, 823

Tielens, A. G. G. M., Meixner, M. M., van der Werf, P. P., Bregman, J., Tauber, J. A. et al. 1993, Sci, 262, 86

Tokunaga, A. T. 1984, AJ 89, 172

Tully, R. B. 1988, *Catalog of Nearby galaxies* (Cambirdge: Cambridge University Press)

Vacca, W. D., Conti, P. S. 1992, ApJ 401, 543

de Vaucouleurs, G., de Vaucouleurs, A., Corwin, H. G., Buta, R. J., Paturel, G., Fouqué, P. 1991, *Third Reference Catalog of Galaxies*, (New-York: Springer Verlag)

Viallefond, F., Thuan, T. X. 1983, ApJ 269, 444

Vigroux, L., Mirabel, F., Altieri, B., Boulanger, F., Cesarsky, C. et al. 1996, A&A, 315, L93